Contrasting intra- and extracellular distribution of catalytic ferrous iron in ovalbumin-induced peritonitis

Fumiya Ito [a], Takahiro Nishiyama [a, b], Lei Shi [a], Masahiko Mori [a, c], Tasuku Hirayama [d], Hideko Nagasawa [d], Hiroyuki Yasui [e], Shinya Toyokuni [a, *]

[a] Department of Pathology and Biological Responses, Nagoya University Graduate School of Medicine, 65 Tsurumai-cho, Showa-ku, Nagoya 466-8550, Japan
[b] Department of Hematology and Oncology, Nagoya University Graduate School of Medicine, 65 Tsurumai-cho, Showa-ku, Nagoya 466-8550, Japan
[c] Department of Obstetrics and Genecology, Nagoya University Graduate School of Medicine, 65 Tsurumai-cho, Showa-ku, Nagoya 466-8550, Japan
[d] Laboratory of Pharmaceutical and Medical Chemistry, Gifu Pharmaceutical University, 1-25-4 Daigaku-Nishi, Gifu 501-1113, Japan
[e] Department of Analytical and Bionorganic Chemistry, Kyoto Pharmaceutical University, 5 Misasagi-Nakauchi-cho, Yamashina-ku, Kyoto 607-8414, Japan

ARTICLE INFO

ABSTRACT

Iron is an essential nutrient for every type of life on earth. However, excess iron is cytotoxic and can lead to an increased cancer risk in humans. Catalytic ferrous iron [Fe(II)] is an initiator of the Fenton reaction, which causes oxidative stress by generating hydroxyl radicals. Recently, it became possible to localize catalytic Fe(II) *in situ* with a turn-on fluorescent probe, RhoNox-1. Here, we screened each organ/cell of rats to globally evaluate the distribution of catalytic Fe(II) and found that eosinophils showed the highest abundance. In various cells, lysosomes were the major organelle, sharing ~40–80% of RhoNox-1 fluorescence. We then used an ovalbumin-induced allergic peritonitis model to study the dynamics of catalytic Fe(II). Peritoneal lavage revealed that the total iron contents per cell were significantly decreased, whereas an increase in the number of inflammatory cells (macrophages, neutrophils, eosinophils and lymphocytes) resulted in an increased total iron content of the peritoneal inflammatory cells. Notably, macrophages, eosinophils and neutrophils exhibited significantly increased catalytic Fe(II) with increased *DMT1* expression and decreased *ferritin* expression, though catalytic Fe(II) was significantly decreased in the peritoneal lavage fluid. In conclusion, catalytic Fe(II) *in situ* more directly reflects cellular activity and the accompanying pathology than total iron does.

1. Introduction

No living thing on earth can survive without iron, but iron is a double-edged sword. Whereas deficiency causes anemia, the excess of iron is a risk for cancer and other various diseases in higher animals [1–3]. Over the past two decades, studies have revealed various novel molecules that are associated with iron absorption and transfer as well as their regulation at the transcriptional, post-transcriptional and protein degradation levels [4,5].

Because there is no active pathway to excrete iron from higher animals, local or global excess iron is observed in various different pathologies, including bacterial/viral infection, foreign body exposure [6], autoimmunity-associated inflammation and repeated hemorrhage in closed space [7]. Though distinct molecular mechanisms are involved in each case, catalytic (labile) ferrous iron, i.e., Fe(II), has been considered an initiator of the Fenton reaction, which generates the most reactive chemical species, hydroxyl radicals, *in vivo* [8]. Although the detection of oxidatively modified products became available during the 1980s and 1990s [9], the detection of catalytic Fe(II) *in situ* was not previously available.

In 2013, Hirayama et al. developed a fluorescent probe, RhoNox-1, to specifically detect catalytic Fe(II) [10], and we showed its applicability to frozen sections [11] based on a ferric nitrilotriacetate-induced renal carcinogenesis model [12–14]. Here, we comprehensively stained tissues in rats with RhoNox-1, which revealed that eosinophils have the highest level of catalytic Fe(II). Further experiments using ovalbumin (OVA) in a rat peritonitis model revealed a distinct altered distribution of catalytic Fe(II) in inflammatory cells.

* Corresponding author.
  E-mail address: toyokuni@med.nagoya-u.ac.jp (S. Toyokuni).

2. Materials and methods

2.1. Reagents

RhoNox-1 was synthesized as described [10], preserved at −80 °C until use, and dissolved in dimethyl sulfoxide to produce a 10 mM solution. It was further diluted with 10 mM phosphate-buffered saline (pH 7.2; PBS) and was used within a single day.

2.2. Animal experiments

The animal experiment committee of Nagoya University Graduate School of Medicine approved the following experiments. Fischer-344 rats were obtained from SLC Japan (Shizuoka, Japan). The OVA-induced allergic peritonitis model was produced as previously described [15–17]. Briefly, male Fischer-344 rats (6 weeks; 140–150 g body weight) were injected with an intraperitoneal injection of a mixture of 1 mg OVA (Thermo Fisher Scientific, Waltham, MA, USA) and 25 mg Alum (Sigma-Aldrich, St. Louis, MO, USA) three times for 3 consecutive days. Three weeks after sensitization, the rats were injected intraperitoneally with 1 mg OVA only (Fig. 1A). We collected peripheral blood (PB) and peritoneal lavage [PL; 30 ml physiological saline, containing 200 μM tris (2-pyridylmethyl) amine (Sigma Aldrich)] 48 h after the final exposure as previously described [18]. PB was analyzed with VetScan HM5 (Abaxis; Union City, CA, USA). PL samples underwent centrifugation (720 × g, 5 min) to collect cells, to which RhoNox-1 was added to a final concentration of 10 μM; the samples were then incubated for 1 h at 37 °C and analyzed with PowerScan4 (DS Pharma Biomedical, Osaka, Japan).

2.3. Histological detection of catalytic Fe(II)

Untreated control or peritonitis model rats were euthanized at 7–9 weeks of age. Each organ was dissected and embedded in Tissue-Tek OCT compound (Sakura Finetek, Torrance, CA, USA) with dry ice-cooled acetone as previously described [11]. Briefly, frozen sections of 8-μm thickness were prepared with a cryostat on a glass slide, fixed in 20% formalin in methanol for 3 min and washed with PBS five times. Then, 200 μl of 10 μM RhoNox-1 was placed on the specimens and incubated for 30 min at 37 °C in a dark chamber, followed by counterstaining with Hoechst33342 (Thermo Fisher) and observation with a fluorescence microscope (BZ-9000; Keyence, Osaka, Japan). It was possible to preserve the frozen sections prior to RhoNox-1 reaction at 4 °C for at least 24 h after cutting. For the quantitation of catalytic Fe(II), each image was divided into RGB elements, to which the ImageJ version 1.47 software (http://www.rsb.info.nih.gov/ij/) was applied: the blue component was used for the nucleus, and the red component was used to examine catalytic Fe(II). Integration of the red color (RhoNox-1) divided by the number of nuclei in the analyzed area with a 100× oil-immersion objective lens was calculated as arbitrary units (AU). At least three random areas were selected for each analysis.

2.4. Flow cytometry and cell sorting

Collected cells from Section 2.2 were rinsed by RPMI1640 without phenol red (Wako, Osaka, Japan), centrifuged (720 × g, 5 min) and suspended in 1-ml RPMI1640 without phenol red. The cells were counted with a hemocytometer. RhoNox-1 solution (final concentration 10 μM) was added to a tube containing cells and incubated in the dark at 37 °C for 30 min, after which Hoechst33342 (final concentration 100 μM) was added. After 30 min, the cells were centrifuged (180 × g, 5 min) and suspended in Hank's Balanced Salt Solution (HBSS) without phenol red (Wako). Cell analysis and sorting were carried out using FACS Aria II (BD Biosciences; San Jose, CA, USA). At first, Hoechst33342-negative cells were removed as dead cells. We observed 4 subsets of living cells with forward scatter (FSC) and side scatter (SSC), each of which was sorted (post-sorting purity > 90%) and underwent iron measurement analysis. Hoechst33342 and RhoNox-1 were excited by 375 nm and 488 nm, respectively. Fluorescent signals were measured at 450 nm (450/50) for Hoechst33342 and at 575 nm (575/30) for RhoNox-1. All flow cytometric data were analyzed using FACSDiva version 8.0.1.

2.5. Cell culture experiments

The HL-60 leukemia cell line and IMR-90-SV human fibroblast cell line, derived from embryonic tissue with SV40 immortalization, were from RIKEN CELL BANK (Ibaragi, Japan). The Met5A human mesothelial cell line, with SV40 transformation, was from ATCC (Manassas, VA, USA), and the NHLF human fibroblast cell line was from Lonza (Walkersville, MD, USA). RPMI1640, containing 10% fetal bovine serum (Biowest, #S1820; Nuaillé, France) and 1% antibiotic-antimyocotic (Gibco, #15240-062; Grand Island, NY, USA), was used in a humidified incubator at 37 °C with 5% CO_2. The cells were used within two months after thawing. Phorbol 12-myristate 13-ascetate (PMA; Wako) was diluted to 160 μM with acetone and preserved at −20 °C. HL-60 cells were incubated with 16 nM PMA for 48 h for differentiation into macrophages [19].

2.6. Western blotting

The cells were lysed with a lysis buffer (1 M NaCl, 50 mM Tris-HCl, 0.1% SDS, pH 8.0, 0.5% sodium deoxycholate and 1% NP-40) supplemented with a protease inhibitor cocktail (Roche; South San Francisco, CA, USA). Protein extraction, sodium dodecyl sulfate-polyacrylamide gel electrophoresis (SDS-PAGE) and immunoblot analyses were performed as previously described [20], using anti-DMT-1 rabbit polyclonal antibody (Santa Cruz Biotechnology, sc-30120; Dallas, TX, USA) at a 1:1000 dilution; anti-TfR mouse monoclonal antibody (Thermo Fisher Scientific, 13–6800) at 1:1000; anti-SLC40A1 (ferroportin) rabbit polyclonal antibody (Abcam, ab58695; Cambridge, UK) at 1:500; anti-ferritin light chain rabbit polyclonal antibody (Abcam, ab69089) at 1:1000; anti-ferritin heavy chain rabbit polyclonal antibody (Santa Cruz Biotechnology, sc-25617) at 1:200; and anti-β-actin mouse monoclonal antibody (Sigma-Aldrich) at 1:2000.

2.7. Intracellular localization of catalytic Fe(II)

For fluorescent confocal microscopy, cells were plated on 35-mm glass-bottom dishes, maintained in phenol red-free medium without FBS and imaged through a 100× oil immersion objective lens on a LSM 880 microscope (Carl Zeiss, Oberkochen, Germany). HL-60, NHLF, IMR-90-SV and Met5A were incubated with 10 μM RhoNox-1 and LysoTracker® Green DND-26 (200 nM) (Thermo Fisher Scientific) for 1 h at 37 °C. After incubation, the cells were washed with RPMI1640 without phenol red and incubated with 25 nM MitoTracker® Deep Red FM (Thermo Fisher Scientific) and 100 nM ERTracker™ Blue-White DPX (Thermo Fisher Scientific). The medium was changed to FluoroBrite™ DMEM (Thermo Fisher Scientific), and a Zeiss 880 equipped with a laser diode, an argon laser, a DPSS Laser and a HeNe Laser was used. ERTracker was excited with 405 nm, LysoTracker with 488 nm, RhoNox-1 with 561 nm and MitoTracker with 640 nm, using the standard beam splitter setting.
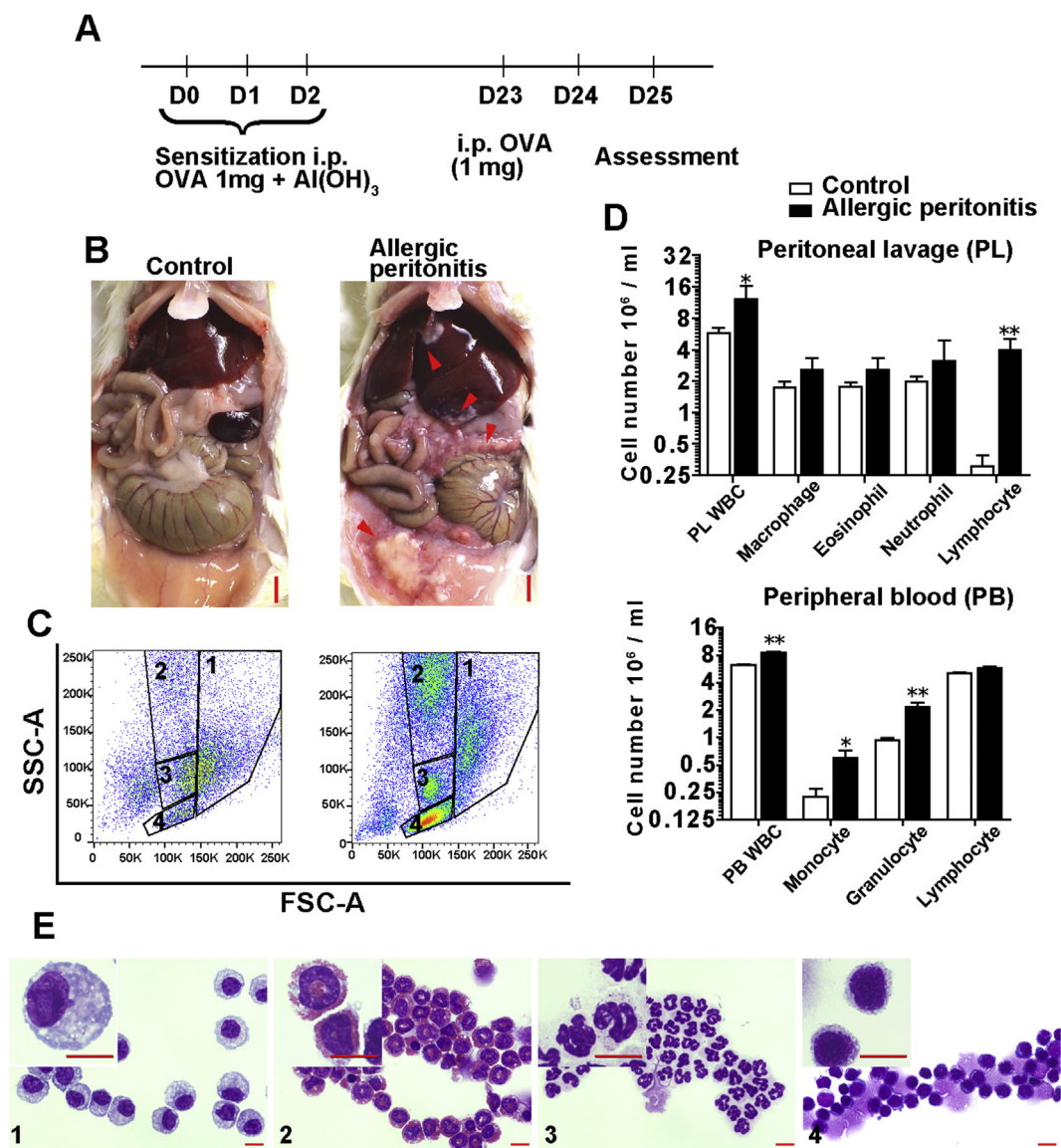
Fig. 1. Inflammatory cells in ovalbumin-induced allergic peritonitis in rats. (A) Protocol. Ovalbumin (OVA) (1 mg) and aluminum hydroxide (Alum) (25 mg) were used for sensitization by intraperitoneal (i.p.) injection, which was followed by i.p. OVA (1 mg) challenge 3 weeks later. (B) Rat peritoneal cavity; untreated control (left) and OVA-induced allergic inflammation (right). Red arrowheads indicate granuloma (bar = 1 cm). (C) Representative corresponding flow cytometric density plot of side scatter (SSC) and forward scatter (FSC) of peritoneal lavage. 1–4 corresponds to 1–4 in E. (D) Cell counts of peritoneal lavage (PL; upper panel) and peripheral blood (PB; lower panel) cell numbers are shown in each model rat. (E) Each subset labelled 1 to 4 was sorted out (1: macrophage; 2: eosinophil; 3: neutrophil; 4: lymphocyte) and stained with May-Grünwald Giemsa (bar = 10 μm; *p < 0.05, **p < 0.01, ***p < 0.001; means ± SEM; N ≥ 6).

2.8. Determination of metal concentration with inductively coupled plasma-mass spectrometry

Collected cells ($1.5-5.0 \times 10^5$/ml) from Section 2.3 were preserved at $-20\,°C$ until analysis. The measurements were performed as previously described [21,22] by inductively coupled plasma-mass spectrometry (ICP-MS; 7700 Series Agilent Technologies; Santa Clara, CA, USA). Six replicates per sample were used for iron, copper, zinc and calcium. The concentration of metal in each sample was calculated from a liner regression of each metal standard curve using standard metal solutions (Wako). Each metal standard curve exhibited regression in the range of 1–500 ng/ml (r = 0.999).

2.9. Determination of catalytic Fe(II) in aqueous sample

Catalytic Fe(II) in an aqueous sample was measured as previously described [11] with slight modifications. The addition of tris(2-pyridylmethy)amine (Sigma-Aldrich; final concentration 200 μM) was used to stabilize Fe(II) in its physiological state. The standard curve is shown (Fig. S1) using ferrous sulfate heptahydrate (Wako).

2.10. Statistical analysis

Statistical analyses were performed using one-way analysis of variance (ANOVA), an unpaired *t*-test and Spearman's rank correlation coefficient with GraphPad Prism 5 software (Graphpad Software, La Jolla, CA, USA). Differences were considered significant
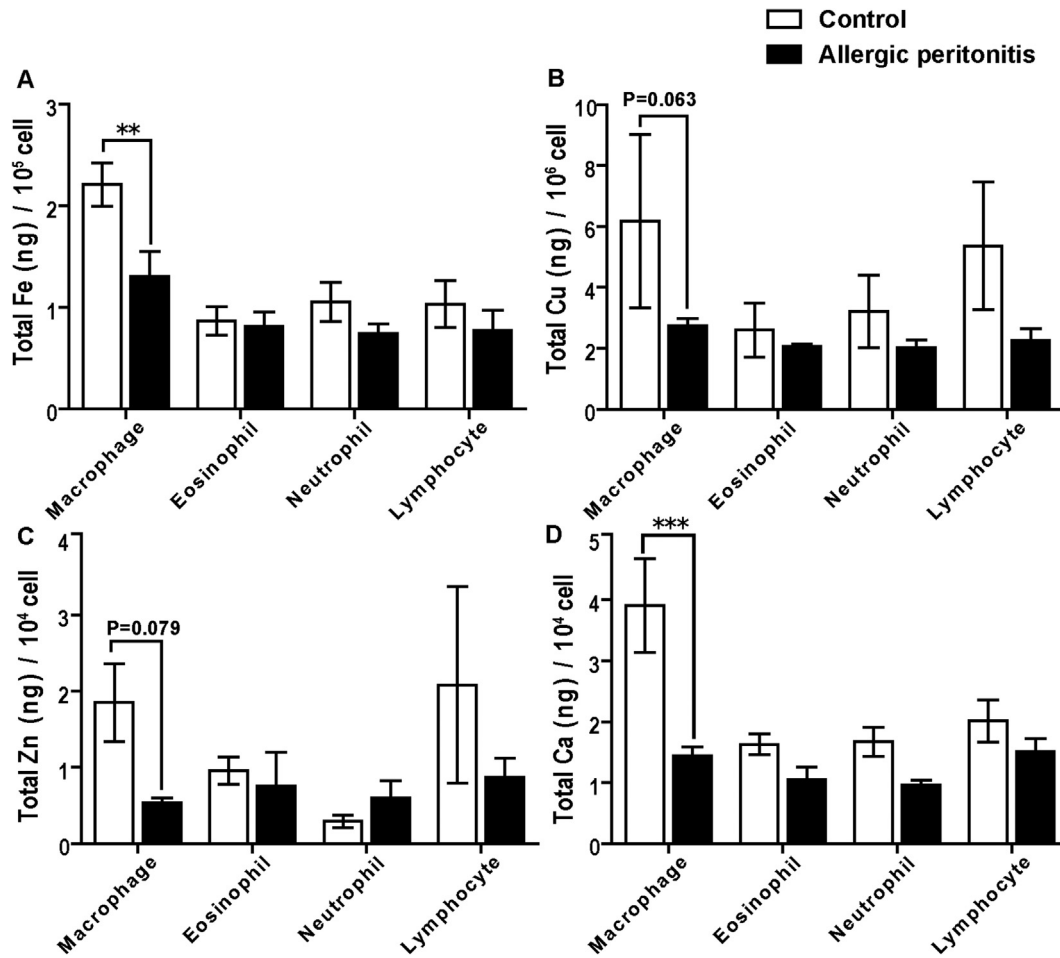
Fig. 2. Measurement of total metals in inflammatory cells (IFCs) of peritoneal lavage. Fractions in Fig. 1B were sorted out using FACS Aria2, which separated the macrophage, eosinophil, neutrophil and lymphocyte subsets. (A) Total iron; (B) total copper; (C) total zinc; (D) total calcium (*p < 0.05, **p < 0.01, ***p < 0.001; means ± SEM; N ≥ 6).

when P < 0.05. The data are expressed as the means ± SEM (n = 3–6) unless otherwise specified. All experiments were repeated at least three times.

3. Results

3.1. Eosinophils harbor the highest levels of catalytic Fe(II) in control rats

Using frozen sections, we stained all of the major rat organs with RhoNox-1. Most of the cells were stained despite different intensities, and we could classify the staining into three distinct patterns: localized, diffuse and extracellular (Fig. S2A). A localized pattern indicates cytoplasmic staining with a granular and/or biased pattern, either apical or basal, and included eosinophils, pancreatic acinar cells and salivary serous glandular cells; a diffuse pattern included cardiac muscle cells, hepatocytes, and duodenal absorptive cells; an extracellular pattern included the epidermal corneal layer, arterial internal elastic lamina, and bronchial submucosa (Fig. S2B). In no case were nuclei stained. Among the cells studied in normal Fischer-344 rats, eosinophils exhibited the highest fluorescent signal, especially in the granules. Thus, we decided to focus on various inflammatory cells. The levels of catalytic Fe(II) in cells other than eosinophils were not significantly different (Fig. S2C).

3.2. OVA-induced allergic peritonitis model and sorting of inflammatory cells in peritoneal lavage

The rat OVA-induced allergic peritonitis model revealed redness, swelling and the adhesion of the intestine and mesentery, concomitant with granuloma formation (Fig. 1B). The corresponding peritoneal lavage was separated into 4 subsets of each cell type via FACS using forward and side scatters (Fig. 1C). Each inflammatory cell increased in number after OVA challenge both in peritoneal lavage and in peripheral blood (Fig. 1D). In peritoneal lavage, lymphocytes increased most in number (Fig. 1D). After the purification of inflammatory cells with FACS cell sorting, each subset was confirmed with May-Grünwald Giemsa staining (Fig. 1E). The cellular purity of each fraction was >90%.

3.3. Macrophages play a role in iron metabolism in OVA-induced allergic peritonitis

In controls, macrophages harbored the highest levels for the total amount of metals examined (Fe, Cu, Zn and Ca). However, the total iron per macrophage cell was significantly decreased in allergic inflammation, as were Cu, Zn and Ca (Fig. 2A-D). The other inflammatory cells (eosinophils, neutrophils and lymphocytes) did not show significant changes in the total amount of each metal per cell. Considering the cell numbers, the total amounts of iron in each
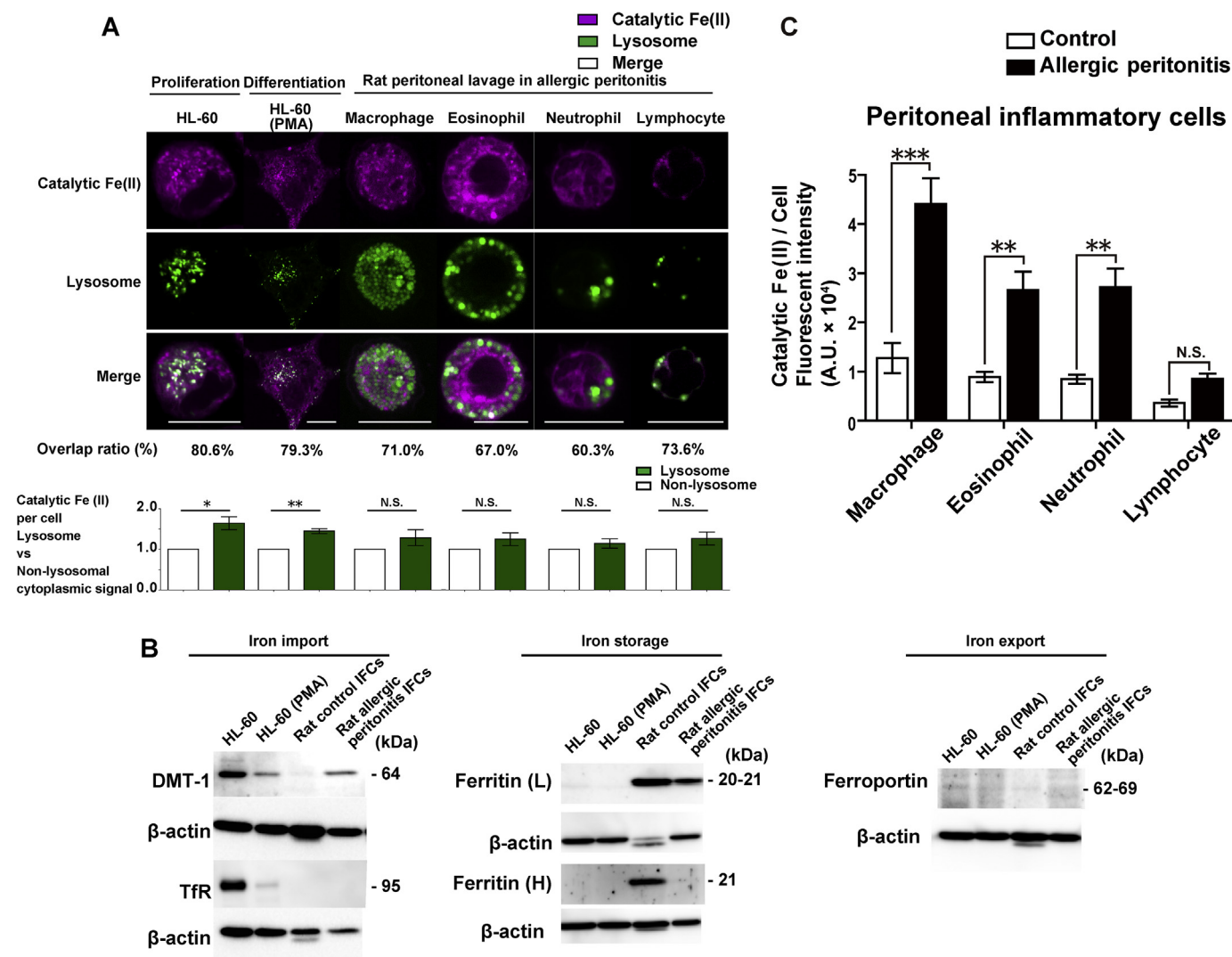
Fig. 3. Intracellular localization of catalytic Fe(II) and its association with function in iron metabolism. (A) Frequent co-localization of catalytic Fe(II) with lysosomes (upper left panels). HL-60 cells were differentiated into promonocytes with phorbol-12-myristate-13-acetate (PMA). Overlap of catalytic Fe(II) with lysosomes was normalized and analyzed with ZEN2 LSM7 co-localization and calculated with Manders' overlap coefficient [29]. Intensity of catalytic Fe(II) was compared between lysosomes and the remainder of the cytoplasm (lower panel). (B) Western blot analysis; DMT-1, transferrin receptor (TfR), ferritin light chain (L), ferritin heavy chain (H) and ferroportin. IFCs, all inflammatory cells. (C) Catalytic Fe(II) in each of the IFCs, separated by FACS Aria2 ($^*p < 0.05$, $^{**}p < 0.01$, $^{***}p < 0.001$; means $\pm$ SEM; N $\geq$ 5).

type of inflammatory cells except macrophages were increased, thus suggesting a role of macrophages as an iron reservoir in normal conditions (Table S1).

3.4. Major fraction of catalytic Fe(II) is localized to lysosomes

The intracellular catalytic Fe(II) could be classified with confocal microscopy into three distinct patterns: fine granular (lysosome, mitochondria), coarse granular (mitochondria, endoplasmic reticulum) and diffuse (cytosol). By co-localization analysis, lysosomes revealed the highest (~60–70%) signal of catalytic Fe(II), followed by mitochondria, endoplasmic reticulum and cytosol or other organelles in non-tumorous cell lines of fibroblasts and mesothelial cells (NHLF, IMR-90-SV and Met5A) (Fig.S3AB). A leukemia cell line, HL-60, revealed a higher localization of catalytic Fe(II) to lysosomes (~80%), regardless of whether the cells were undifferentiated or differentiated to macrophages with PMA stimulation (Fig. 3A). Differentiated HL60 showed lower protein levels of *DMT1* [Fe(II) transporter from lysosome to cytosol] and *TfR* (transferrin receptor)

with lower catalytic Fe(II) signals (Fig. 3AB). The iron storage, as observed by the protein levels of ferritin heavy/light chains, was high in normal peritoneal inflammatory cells. However, the protein levels of both genes were significantly decreased in the peritoneal inflammatory cells of allergic peritonitis, in which the distribution of catalytic Fe(II) in the cytoplasmic non-lysosomal area was increased. Here, the protein levels of DMT-1 were increased, whereas those of ferroportin were low and unchanged (Fig. 3B).

3.5. Catalytic Fe(II) is increased in inflammatory cells but is decreased in peritoneal lavage fluid in OVA-induced allergic peritonitis

In allergic inflammation, catalytic Fe(II) in the peritoneal lavage fluid (85.6 $\pm$ 36.7 nM; mean $\pm$ SEM, N = 5) was significantly lower than for the untreated control (391.3 $\pm$ 36.3 nM, N = 5; p < 0.001). In contrast, the intracellular catalytic Fe(II) in inflammatory cells other than lymphocytes was significantly increased in allergic peritonitis, including for macrophages, which revealed the most

marked increase (Fig. 3C).

4. Discussion

After our application of RhoNox-1 probe to frozen sections [11], in the present study we screened for cells with high catalytic Fe(II) in normal rats and found that eosinophils reveal the highest catalytic Fe(II). Because eosinophilic inflammation is occasionally associated with anemia [23] and eosinophils are intimately associated with allergic inflammation [24], we undertook a study to determine the dynamics of iron and catalytic Fe(II) in OVA-induced allergic peritonitis in rats.

Among the total amounts of metals examined (Fe, Zn, Cu and Ca), iron was the only metal that significantly changed in its amounts per cell and significantly decreased in macrophages. Considering the increased number of inflammatory cells in the peritoneal cavity in allergic peritonitis, the share of iron in macrophages decreased from ~50% to ~30%, despite the total iron increase of ~40% in all inflammatory cells. This increase was shared by eosinophils, neutrophils and lymphocytes, with lymphocytes showing a >10-fold increase. This result mainly depends on the increase in the cell number itself.

In sharp contrast, the catalytic Fe(II) was significantly increased in all the inflammatory cells examined. Lysosomes were the major sites for all the cells examined as expected [2], but non-lysosome cytoplasm was also stained with RhoNox-1, which was higher in inflammatory cells. Protein analysis of the total peritoneal inflammatory cells indicates that these cells are devoid of transferrin receptor but store iron in ferritin, which is significantly decreased upon inflammation, with increases in catalytic Fe(II). High levels of DMT1 with low levels of ferroportin suggest the transfer of catalytic Fe(II) from lysosome to cytosol. We suspect that catalytic Fe(II) is used for functional activity, including cellular movement, phagocytosis or cytokine production. Of note, the catalytic Fe(II) in peritoneal lavage fluids was significantly lower than in the control, despite an increase in ascites and inflammatory cells. This result is consistent with the pathologic situation, similar to bacterial infections, where feeding bacteria with iron must be avoided [25,26]. Our findings may be linked to recent reports on the association of the NLRP3 inflammasome with intracellular ferrous iron [27] or aluminum adjuvants [28]. Further studies on organelles other than lysosomes would clarify the precise functional role of catalytic Fe(II) during inflammation.

In conclusion, catalytic Fe(II) is significantly increased in inflammatory cells in OVA-induced allergic peritonitis, and RhoNox-1 is a useful tool to analyze iron metabolism in different pathologies.

Acknowledgements

Transparency document

Transparency document related to this article can be found online at http://dx.doi.org/10.1016/j.bbrc.2016.06.003.

Appendix A. Supplementary data

Supplementary data related to this article can be found at http://dx.doi.org/10.1016/j.bbrc.2016.06.003.

References

[1] S. Toyokuni, Iron-induced carcinogenesis: the role of redox regulation, Free Radic. Biol. Med. 20 (1996) 553–566.

[2] S. Toyokuni, Role of iron in carcinogenesis: Cancer as a ferrotoxic disease, Cancer Sci. 100 (2009) 9–16.

[3] S. Toyokuni, Iron as a target of chemoprevention for longevity in humans, Free Radic. Res. 45 (2011) 906–917.

[4] M.W. Hentze, M.U. Muckenthaler, N.C. Andrews, Balancing acts: molecular control of mammalian iron metabolism, Cell 117 (2004) 285–297.

[5] S.V. Torti, F.M. Torti, Iron and cancer: more ore to be mined, Nat. Rev. Cancer 13 (2013) 342–355.

[6] Y. Wang, Y. Okazaki, L. Shi, H. Kohda, M. Tanaka, K. Taki, T. Nishioka, T. Hirayama, H. Nagasawa, Y. Yamashita, Role of hemoglobin and transferrin in multi-wall carbon nanotube-induced mesothelial injury and carcinogenesis, Cancer Sci. 107 (2015) 250–257.

[7] M. Mori, F. Ito, L. Shi, Y. Wang, C. Ishida, Y. Hattori, M. Niwa, T. Hirayama, H. Nagasawa, A. Iwase, Ovarian endometriosis-associated stromal cells reveal persistently high affinity for iron, Redox Biol. 6 (2015) 578–586.

[8] S. Toyokuni, Reactive oxygen species-induced molecular damage and its applicaton in pathology, Pathol. Int. 49 (1999) 91–102.

[9] S. Toyokuni, The origin and future of oxidative stress pathology: from the recognition of carcinogenesis as an iron addiction with ferroptosis-resistance to non-thermal plasma therapy, Pathol. Int. 66 (2016) 245–259.

[10] T. Hirayama, K. Okuda, H. Nagasawa, A highly selective turn-on fluorescent probe for iron(II) to visualize labile iron in living cells, Chem. Sci. 4 (2013) 1250–1256.

[11] T. Mukaide, Y. Hattori, N. Misawa, S. Funahashi, L. Jiang, T. Hirayama, H. Nagasawa, S. Toyokuni, Histological detection of catalytic ferrous iron with the selective turn-on fluorescent probe RhoNox-1 in a Fenton reaction-based rat renal carcinogenesis model, Free Radic. Res. 48 (2014) 990–995.

[12] S. Okada, Y. Minamiyama, S. Hamazaki, S. Toyokuni, A. Sotomatsu, Glutathione cycle dependency of ferric nitrilotriacetate-induced lipid peroxidation in mouse proximal renal tubules, Arch. Biochem. Biophys. 301 (1993) 138–142.

[13] Y. Nishiyama, H. Suwa, K. Okamoto, M. Fukumoto, H. Hiai, S. Toyokuni, Low incidence of point mutations in *H*-, *K*- and *N*-ras oncogenes and p53 tumor suppressor gene in renal cell carcinoma and peritoneal mesothelioma of Wistar rats induced by ferric nitrilotriacetate, Jpn. J. Cancer Res. 86 (1995) 1150–1158.

[14] S. Akatsuka, Y. Yamashita, H. Ohara, Y.T. Liu, M. Izumiya, K. Abe, M. Ochiai, L. Jiang, H. Nagai, Y. Okazaki, H. Murakami, Y. Sekido, E. Arai, Y. Kanai, O. Hino, T. Takahashi, H. Nakagama, S. Toyokuni, Fenton reaction induced cancer in wild type rats recapitulates genomic alterations observed in human cancer, PLoS ONE 7 (2012) e43403.

[15] C. Zuany-Amorim, C. Creminon, M.C. Nevers, M.-A. Nahori, B.B. Vargaftig, M. Pretolani, Modulation by IL-10 of antigen-induced IL-5 generation, and CD4+ T lymphocyte and eosinophil infiltration into the mouse peritoneal cavity, J. Immunol. 157 (1996) 377–384.

[16] A.M. Das, R.J. Flower, M. Perretti, Eotaxin-induced eosinophil migration in the peritoneal cavity of ovalbumin-sensitized mice: mechanism of action, J. Immunol. 159 (1997) 1466–1473.

[17] C.C. Dong, X.J. Yin, J.Y.C. Ma, L. Millecchia, M.W. Barger, J.R. Roberts, X.-D. Zhang, J.M. Antonini, J.K.H. Ma, Exposure of brown Norway rats to diesel exhaust particles prior to ovalbumin (OVA) sensitization elicits IgE adjuvant activity but attenuates OVA-induced airway inflammation, Toxicol. Sci. 88 (2005) 150–160.

[18] C. Zuany-Amorim, D. Leduc, B.B. Vargaftig, M. Pretolani, Characterization and pharmacological modulation of antigen-induced peritonitis in actively sensitized mice, Br. J. Pharmacol. 110 (1993) 917–924.

[19] G. Rovera, D. Santoli, C. Damsky, Human promyelocytic leukemia cells in culture differentiate into macrophage-like cells when treated with a phorbol diester, Proc. Natl. Acad. Sci. U. S. A. 76 (1979) 2779–2783.

[20] S. Toyokuni, W. Kawaguchi, S. Akatsuka, M. Hiroyasu, H. Hiai, Intermittent microwave irradiation facilitates antigen-antibody reaction in Western blot analysis, Pathol. Int. 53 (2003) 259–261.

[21] H. Nagai, Y. Okazaki, S. Chew, N. Misawa, Y. Yamashita, S. Akatsuka, K. Yamashita, T. Ishihara, Y. Yoshikawa, L. Jiang, H. Ohara, T. Takahashi, G. Ichihara, K. Kostarelos, Y. Miyata, H. Shinohara, S. Toyokuni, Diameter of multi-walled carbon nanotubes is a critical factor in mesothelial injury and subsequent carcinogenesis, Proc. Natl. Acad. Sci. U. S. A. 108 (2011) E1330–E1338.

[22] M. Kume, H. Yasui, Y. Yoshikawa, M. Horinouchi, K. Higashiguchi, Y. Kobayashi, D. Kuroda, T. Hirano, M. Hirai, T. Nakamura, Transient elevation of serum cystatin C concentrations during perioperative cisplatin-based chemotherapy in esophageal cancer patients, Cancer Chemother. Pharmacol. 69 (2012) 1537–1544.

[23] M.E. Rothenberg, Eosinophilic gastrointestinal disorders (EGID), J. Allergy Clin. Immunol. 113 (2004) 11–28.

[24] P.C. Fulkerson, M.E. Rothenberg, Targeting eosinophils in allergy, inflammation and beyond, Nat. Rev. Drug Discov. 12 (2013) 117–129.

[25] E.P. Skaar, The battle for iron between bacterial pathogens and their vertebrate hosts, PLoS Pathog. 6 (2010) e1000949.

[26] R. Saha, N. Saha, R.S. Donofrio, L.L. Bestervelt, Microbial siderophores: a mini review, J. Basic Microbiol. 53 (2013) 303–317.

[27] K. Nakamura, T. Kawakami, N. Yamamoto, M. Tomizawa, T. Fujiwara, T. Ishii, H. Harigae, K. Ogasawara, Activation of the NLRP3 inflammasome by cellular labile iron, Exp. Hematol. 44 (2016) 116–124.

[28] S.C. Eisenbarth, O.R. Colegio, W. O'Connor, F.S. Sutterwala, R.A. Flavell, Crucial role for the Nalp3 inflammasome in the immunostimulatory properties of aluminium adjuvants, Nature 453 (2008) 1122–1126.

[29] K.W. Dunn, M.M. Kamocka, J.H. McDonald, A practical guide to evaluating colocalization in biological microscopy, Am. J. Physiol. Cell Physiol. 300 (2011) C723–C742.